doi: 10.18720/MCE.80.8

Cold-formed RHS T joints with initial geometrical imperfections

Сварные узлы холодногнутых труб прямоугольного сечения с начальными несовершенствами

M. Garifullin*,
Tampere University of Technology, Tampere, Finland
M.K. Bronzova,
Peter the Great St. Petersburg Polytechnic University, St. Petersburg, Russia
M. Heinisuo,
K. Mela,
S. Pajunen,
Tampere University of Technology, Tampere, Finland

Аспирант М.Р. Гарифуллин*,
Технологический университет Тампере, Тампере, Финляндия
студент М.К. Бронзова,
Санкт-Петербургский политехнический университет Петра Великого, г. Санкт-Петербург, Россия
д-р техн. наук, профессор М. Хейнисуо,
канд. техн. наук, старший научный сотрудник К. Мэла,
канд. техн. наук, доцент С. Паюнен,
Технологический университет Тампере, Тампере, Финляндия

Key words: hollow section joint; resistance; initial stiffness; finite element analysis; imperfection

Ключевые слова: трубный узел; прочность; начальная жесткость; метод конечных элементов; несовершенства

Abstract. Generally, numerical simulations of structures are carried out in such a way as to most accurately repeat their real behavior. The current rules for finite element modeling of tubular joints oblige scientists and engineers to construct their numerical models considering initial imperfections. However, not all joints are sensitive to initial imperfections. Often consideration of initial imperfections brings no reasonable improvements in the accuracy of results, but severely complicates numerical simulations. In such cases, the effect of geometrical imperfections can be effectively replaced by a simple theoretical equation or neglected entirely. This paper evaluates the effect of initial geometrical imperfections on the structural behavior of cold-formed rectangular hollow section T joints. Imperfections are simulated using the conventional approach for thin-walled structures, applying corresponding buckling modes to the perfect geometry. The paper analyzes several buckling modes and their combinations to identify the most rational technique for simulation of imperfections under in-plane bending and axial loading. Based on the obtained results, parametric studies are conducted to investigate the effect of initial imperfections on joints with various geometry and material properties. The results demonstrate that initial imperfections reduce the resistance and initial stiffness of joints. However, the observed effect has been found sufficiently small to be safely ignored in computational analyses.

Аннотация. Как правило, конечно-элементный анализ строительных конструкций проводится таким образом, чтобы максимально точно повторить их реальную работу. Современные требования к конечно-элементному анализу трубных узлов обязывают ученых и инженеров учитывать влияние начальных несовершенств. Однако, как показывает практика, не все узлы чувствительны к начальным несовершенствам. Часто учет несовершенств не позволяет получить более точные результаты, однако серьезно усложняет расчет конструкций. В таких случаях влияние несовершенств может быть учтено простой аналитической формулой или не учитываться вообще. Данная статья исследует влияние начальных геометрических несовершенств на несущую способность Т-образных узлов из труб прямоугольного сечения. Несовершенства моделируются при помощи традиционного для тонкостенных конструкций метода, когда соответствующая форма потери устойчивости узла прикладывается к его идеальной геометрии. Чтобы определить наиболее целесообразный подход к моделированию несовершенств для изгиба в плоскости узла и продольного сжатия, статья анализирует несколько форм потери устойчивости, а также их возможные комбинации. На основании полученных данных статья проводит параметрические исследования, чтобы определить влияние несовершенств на работу узлов с различной геометрией и свойствами стали. Результаты показали, что начальные несовершенства уменьшают несущую способность трубных узлов. Однако наблюдаемый

Гарифуллин М.Р., Бронзова М.К., Хейнисуо М., Мэла К., Паюнен С. Сварные узлы холодногнутых труб прямоугольного сечения с начальными несовершенствами // Инженерно-строительный журнал. 2018. № 4(80). С. 81–94.

негативный эффект достаточно мал и позволяет проводить расчет конструкций без учета влияния геометрических несовершенств.

1. Introduction

To provide most reliable results, numerical simulations are carried out in such a way as to most accurately repeat the real behavior of structures. Generally, the finite element analysis of tubular joints incorporates nonlinear large deflection theory for displacements, a nonlinear elastic-plastic material law as well as initial imperfections [1]. Initial imperfections include the deviations of geometry, imperfections in boundary conditions and residual stresses. Cold-formed tubular welded joints are generally influenced by initial geometrical imperfections, welding residual stresses and the residual stresses that occur from the cold-forming process.

The influence of welding residual stresses on structural behavior of rectangular hollow section joints was investigated in [2, 3] and was found negligible. Residual stresses in tubular joints obtained from cold-forming process were studied in [4–6]. However, very limited research is dedicated to studying initial geometrical imperfections in tubular joints. Most of the current papers conduct finite element analyses ignoring deviations in geometry of tubular members [7–10]. Although such an approach can be fully justified for members with very thick walls, it is not clear, whether or not the same can be assumed for tubes with relatively thin walls. These joints may behave similarly to thin-walled structures, which demonstrate considerable reduction of resistance due to imperfections in geometry [11, 12]. Moreover, the effect of initial imperfections might differ for the joints made of high strength steels, which are known to be particularly sensitive to any uncertainties. If the influence of initial imperfections is considerable, ignoring them in the design of tubular joints can lead to the overestimation of their load-bearing capacity, leading thus to unsafe results.

This paper investigates numerically the effect of initial geometrical imperfections on the resistance and initial stiffness of rectangular hollow section (RHS) T joints. A T joint represents the simplest joint configuration, when a brace is welded to a chord at an angle of 90°, as shown in Figure 1a. Section 2 develops the finite element (FE) model for RHS T joints and briefly describes its structural behavior under in-plane bending M_{ip} and axial brace loading N. The loading cases are demonstrated in Figure 1b. Initial imperfections are modelled by applying the scaled buckling modes to perfect geometry. Section 3.1 considers various buckling modes and their combinations by comparing the structural behavior of perfect and imperfect FE models. Finally, Section 3.2 provides parametric studies of RHS T joints with varying geometry and steel grades. The paper investigates only butt-welded joints, with no welding imperfections considered.

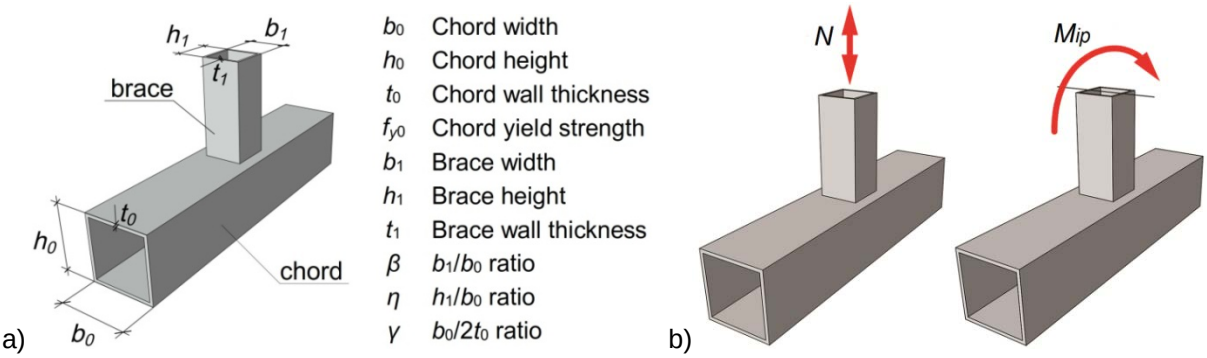

Figure 1. RHS T joint: a) notations; b) loading cases

2. Methods

2.1. Development of FE model

The FE model for RHS T joints under in-plane bending was developed in [13]. This paper conducts numerical analyses employing the FE package Abaqus/Standard [14]. Cold-formed sections were modeled with round corners, according to EN 10219-2:2006 [15]. Residual stresses due to cold-forming were not considered. To exclude the possible effects of chord boundary conditions, its length was selected as $6b_0$, as recommended in [16], while the brace length was chosen as $4b_1$, as shown in Figure 2a. The wall thickness of the brace t_1 was chosen so that it did not exceed the thickness of the chord t_0. Following the recommendations of [17], the sections were modelled using solid quadratic finite

elements with reduced integration (C3D20R), with two elements in the thickness direction. To capture large stress gradients, the mesh was refined near the connection area.

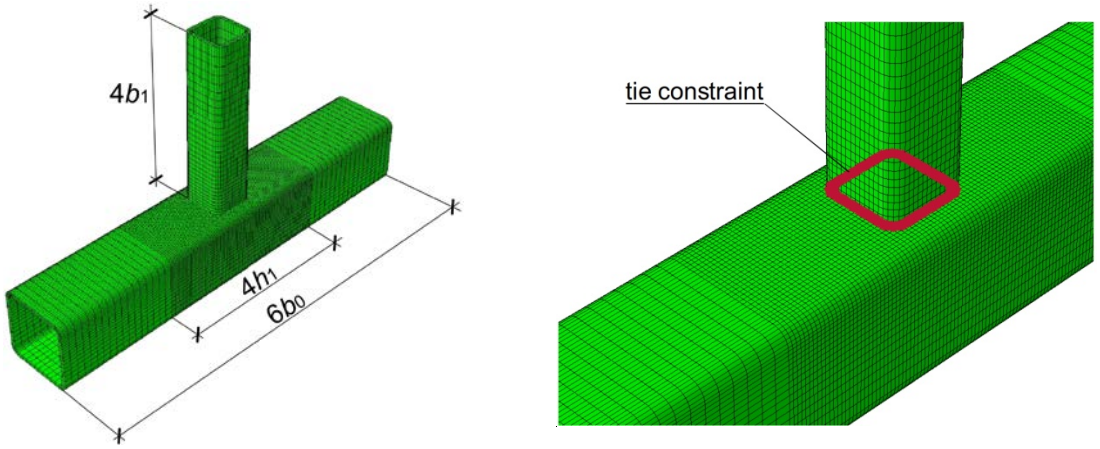

a) b)

Figure 2. FE model: a) meshing; b) welds modeling

The joints were modelled with butt welds, considering them as the continuation of the brace parent material. The connection was simulated using the tie constraint [14], which ties two separate surfaces together with no relative motion between, as shown in Figure 2b. This approach allows using individual meshes for the connected members with no direct matching of their nodes [18]. All calculations employed the elastic-plastic material model with linear strain hardening according to EN 1993-1-5:2006 [19], with the Young's modulus of E = 210 GPa and the Poisson's ratio of v = 0.3, as shown in Figure 3a.

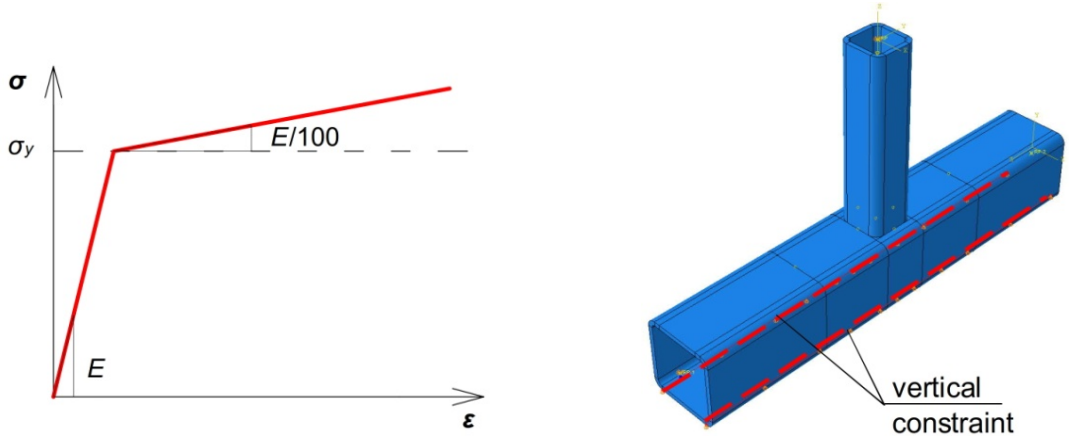

a) b)

Figure 3. a) Material model; b) boundary conditions to prevent bending of the chord

Loading was performed using a force-controlled nonlinear static analysis. The load was applied to the end of the brace by a concentrated in-plane moment M or an axial force N. In case of axial brace loading, the axial force N causes in-plane bending of the chord, producing additional normal stresses on its faces. These stresses affect the structural behavior of tubular joints, reducing their resistance and initial stiffness [20]. To eliminate this effect, the bottom flange of the chord was restrained along the whole length against vertical displacements, as shown in Figure 3b.

2.2. Modeling imperfections

Currently, there are two main approaches for the implementation of geometrical imperfections to the perfect model. The first method represents measuring the real imperfections of members using non-contact 3D deformation scanners [21, 22]. The measured imperfections are then added to the FE model. Such a method provides a very realistic distribution of imperfections along the surface of members but is very time-consuming and is not widely used due to the high price of the measuring equipment.

The second approach is described in Appendix C.5 of EN 1993-1-5:2006 [19] and it represents the simulation of equivalent imperfections. On the first step, a linear buckling analysis is performed. The obtained buckling modes are then scaled and implemented to a model with perfect geometry. The direction of the applied imperfections should be such that the lowest resistance is obtained. Although the resulting distribution of imperfections in this case represents a rather simplified pattern, this straightforward method is widely used, particularly for thin-walled structures [23, 24]. This approach is employed in the present study in all FE analyses. According to EN 1993-1-8:2005 [25], the most typical failure modes for RHS T joints are chord face bending for $\beta \leq 0.85$ and chord side walls failure for $0.85 < \beta \leq 1.0$. This means that local deformations in RHS T joints are generally located in the chord. Therefore, this paper considers geometrical imperfections only in relation to the chord member.

When imperfections are applied based on a linear buckling analysis, attention should be paid on two issues. The first one concerns the shape and the amplitude of imperfections. To apply imperfections in the most unfavorable way, their shape should possibly repeat the deformation pattern of the joint under the corresponding load. Figure 4a shows the typical deformation pattern of the RHS T joint under an axial brace loading. In this case, imperfections can be applied as the concavity of the chord top face x_1 and the convexity of its web x_2. The deformation of the RHS T joint under in-plane bending can be considered as a combination of a compressed and a tensile part. In this case, geometrical imperfections can be applied similarly using the corresponding buckling modes.

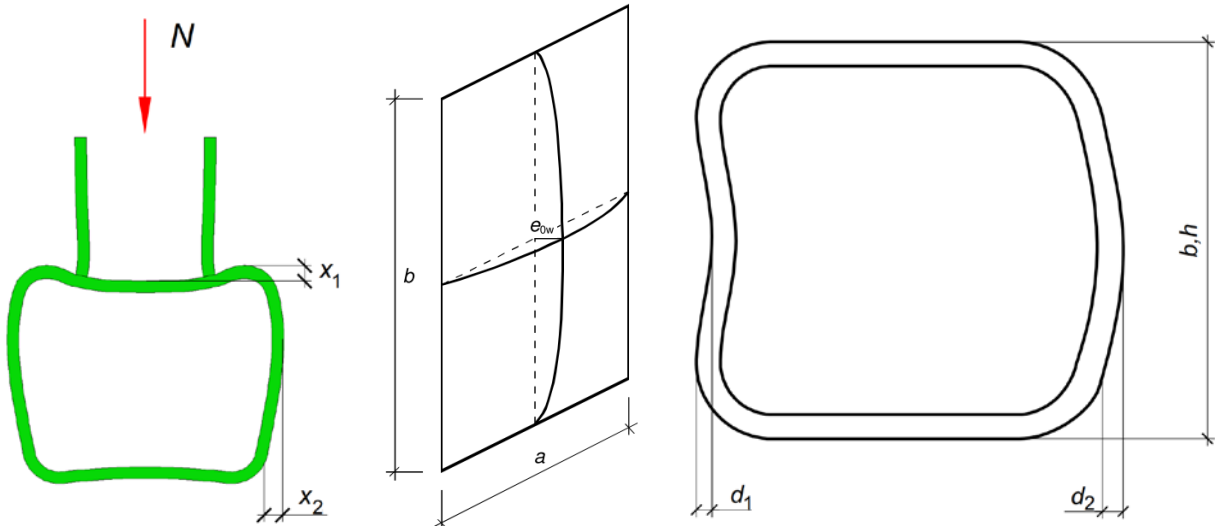

Figure 4. a) Deformation shape of RHS T joint under axial brace loading; b) limitations provided in EN 1993-1-5:2006 [19]; c) limitations provided in EN 10219-2:2006

According to [4], maximum measured imperfections can be conservatively used to predict lower bound strength in the FE analysis. The required magnitudes of imperfections can be found in Eurocode. Appendix C.5 of EN 1993-1-5:2006 [19] specifies local imperfections equal to $e_w = a/200$ or $b/200$, as shown in Figure 4b. In relation to a RHS chord, these values respectively correspond to $b_0/200$ and $h_0/200$. The same amplitudes are used in many publications [26, 27]. Another value can be found in EN 10219-2:2006 [15], which limits the concavity and convexity of cold-formed RHS tubes by 0.8 % with a minimum of 0.5 mm, see d_1 and d_2 in Figure 4c. This corresponds to the values of $b_0/125$ and $h_0/125$. The same limit can be found in [28]. Experimental measurements of the imperfections on hollow sections [5, 29, 30] demonstrate that real imperfections generally do not exceed these amplitudes. This paper employs the values of $b_0/125$ and $h_0/125$, as the most conservative limitations.

The second issue of this approach relates to the combination rules for buckling modes, i.e. the number of buckling modes to be applied and their corresponding scaling factors. Generally, the deformation pattern of the joint is governed by the first buckling mode [4]. However, if the difference between the first and subsequent eigenvalues is small, some subsequent buckling modes can also contribute to the overall deformation. To take into account several buckling modes, a combination rule for their imperfections should be considered. Appendix C of EN 1993-1-5:2006 [19] states that any buckling mode can be taken as the leading imperfection, and the accompanying modes may have their values reduced to 70 %. This leads to the following combination rule:

$$e_0 = e_1 + 0.7\left(e_2 + e_3 + ... + e_n\right), \quad (1)$$

where e_0 is the total amplitude, e_n is the amplitude from buckling mode n, n is the amount of considered buckling modes. It should be noted that the summation should be conducted very thoroughly, paying attention to the shape of buckling modes. Eq. (1) considers the amplitudes at some particular point of interest. This paper considers the imperfections of the chord; therefore, Eq. (1) regulates the convexity of the chord side walls, denoted as x_2 in Figure 4a. Therefore, it should include only those modes that have the maximum (or at least considerable) deformation in the chord side walls. The direction of imperfections is also important: if negative buckling modes are included Eq. (1), they have to be multiplied by negative scaling factors to be applied in the proper direction.

2.3. Structural behavior of RHS T joints

The local beam model for semi-rigid tubular T joints has been developed in [31]. The models under in-plane bending moment and axial brace loading are depicted in Figure 5, where $S_{j,ini}$ and $C_{j,ini}$ denote initial rotational and axial stiffnesses, which are modelled by rotational and linear springs, respectively. It should be noted that the springs are located at the upper flange of the chord and they are connected to the chord axis by a rigid beam.

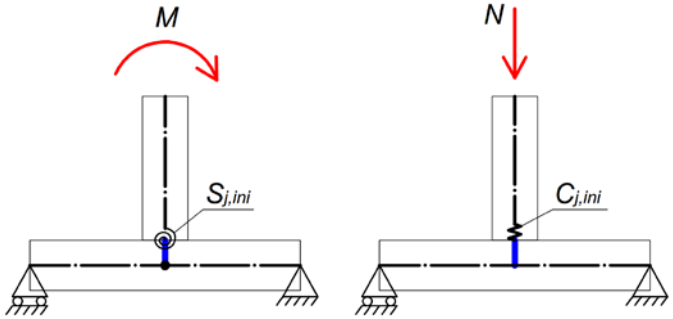

Figure 5. Design local models for RHS T joint: a) in-plane bending; b) axial brace loading

Generally, displacements and rotations measured in a FE analysis reflect the global behavior of the joint, including deformations of the chord and the brace, as well as the local deformations of the joint. The latter represents the deformations at the connection area, where the brace and the chord meet. In particular, to obtain the local rotation of the joint φ in case of in-plane bending, the rotation of the brace φ_{br} and the rotation of the chord φ_{ch} are subtracted from the measured rotation in the end of the brace φ_{tot} (Figure 6):

$$\varphi = \varphi_{tot} - \varphi_{br} - \varphi_{ch} \quad (2)$$

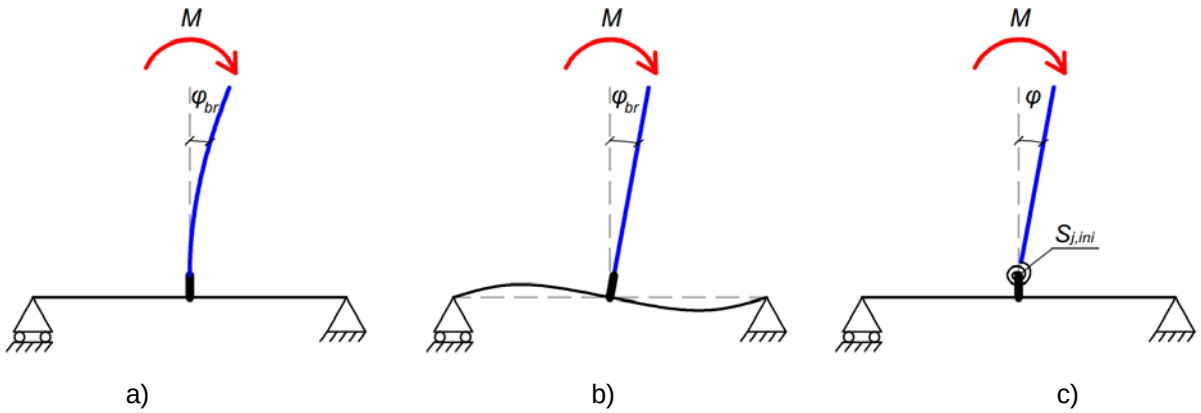

Figure 6. Behavior under in-plane bending: a) elastic rotation of the brace; b) elastic rotation of the chord; c) local rotation of the joint

To obtain local displacements in case of axial loading, the displacement in the end of the brace δ_{tot} is reduced by the brace shortening δ_{sh}:

$$\delta = \delta_{tot} - \delta_{sh}. \quad (3)$$

The motions of the members are supposed to be elastic (assuming that plastic deformations occur only in the connection area); therefore, the values φ_{br}, φ_{ch}, and δ_{sh} are calculated manually using the well-known beam equations from strength of materials:

$$\varphi_{br} = \frac{Ml_1}{EI_1}; \quad \varphi_{ch} = \frac{Ml_0}{12EI_0}; \quad \delta_{sh} = \frac{Nl_1}{EA_1} \quad (4)$$

where l_0 and l_1 are respectively the lengths of the chord and the brace, I_0 and I_1 are respectively the second moments of area of the chord and the brace, A_1 is the cross-sectional area of the brace, E is the Young's modulus.

The structural behavior of tubular joints demonstrates certain similarities in case of in-plane bending and axial brace loading and it is best described by corresponding load-deformation curves. The initial stiffness and resistance of joints are found graphically, using a manual curve-fitting approach. To evaluate the deformation capacity of joints, the 3%b_0 deformation limit is calculated in accordance with [32]. Following this rule, for a joint loaded by an axial brace force, the deformation limit δ_{lim} is found as

$$\delta_{\lim} = 0.03b_0 \quad (5)$$

Similarly, for a joint loaded by an in-plane moment the deformation limit φ_{lim} is

$$\varphi_{\lim} = \frac{0.03b_0}{h_1/2} = \frac{0.06}{\eta} \quad (6)$$

Initial stiffness $S_{j,ini}$ ($C_{j,ini}$) is found as the tangent line in the elastic phase of the curve, as shown in Figure 7. The resistance of joints is determined depending on their brace-to-chord width ratio β [33]. For the joints with $\beta \le 0.85$, bending of the chord top face governs the deformation of the whole joint, and the load-deformation curve has a clearly observed hardening phase, as shown in Figure 7. In this case, plastic resistance M_{pl} (N_{pl}) is determined as the intersection of two tangent lines corresponding to initial stiffness $S_{j,ini}$ ($C_{j,ini}$) and hardening stiffness $S_{j,h}$ ($C_{j,h}$), as demonstrated in [34]. Ultimate resistance M_u (N_u) in this case usually corresponds to very large deformations, considerably exceeding the deformation limit; therefore, it is not considered in this paper.

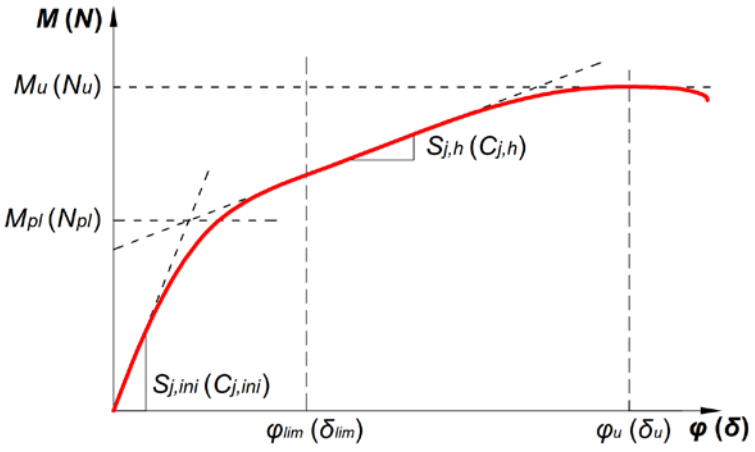

Figure 7. Load-deformation curve for T joint with $\beta \le 0.85$

The behavior of joints with $0.85 < \beta \le 1.0$ is generally governed by chord side walls buckling. Instead of a well-developed hardening phase, the action-deformation curves of such joints have a clear peak load M_{max} (N_{max}). The resistance of such joints depends on the correlation between this peak load and the 3%b_0 deformation limit [35]. If a joint has a peak load M_{max} (N_{max}) at a deformation smaller than φ_{lim} (δ_{lim}), the peak load is considered to be the resistance of the joint, as shown in Figure 8a. If a joint has a peak load M_{max} (N_{max}) at a deformation larger than φ_{lim} (δ_{lim}), resistance is determined as equal to the load at the deformation limit, as shown in Figure 8b.

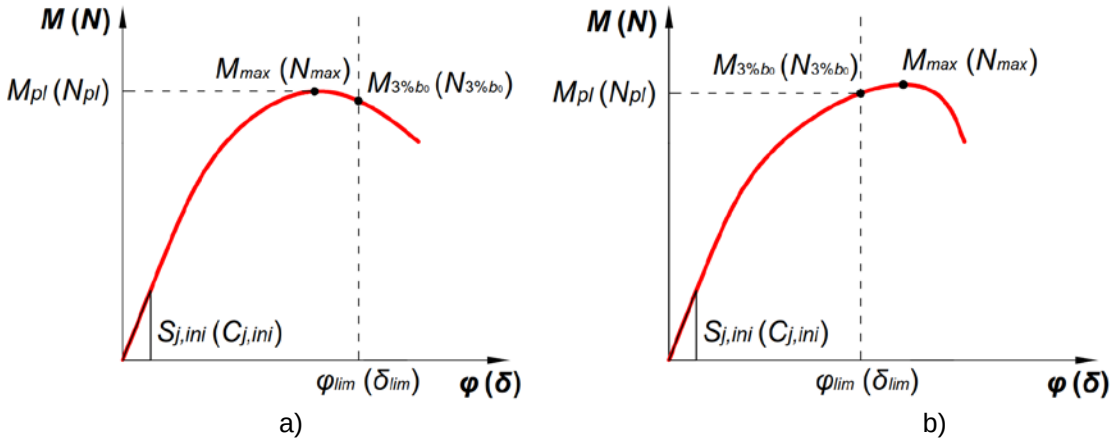

Figure 8. Load-deformation curves for T joint with 0.85 < β ≤ 1.0

3. Results and Discussion

3.1. Influence of initial imperfections on structural behavior of joints

This section investigates the effect of initial geometric imperfections on the structural behavior of RHS T joints under two loading cases: an axial load and an in-plane bending moment. Attention is paid particularly on the buckling modes and their possible combinations that can be used to the proper modeling of imperfections. All analyses were conducted on a single joint with a 100 x 100 x 6 mm chord and a 60 x 60 x 6 mm brace (β = 0.6), made of S355 steel grade.

On the first step, a linear buckling analysis was conducted for the case of in-plane bending and axial brace loading to obtain desired buckling modes. Figure 9 presents the first 10 buckling modes for the case of in-plane bending. As can be seen, Modes 3–10 represent local buckling of the brace and they cannot be applied to simulate chord imperfections. Modes 1 and 2 most closely correspond to the deformation pattern under the moment loading; however, major displacements are observed in the end of the brace, but not in the chord web. For this reason, buckling modes obtained from in-plane bending were found inapplicable for the simulation of imperfections for the considered joint.

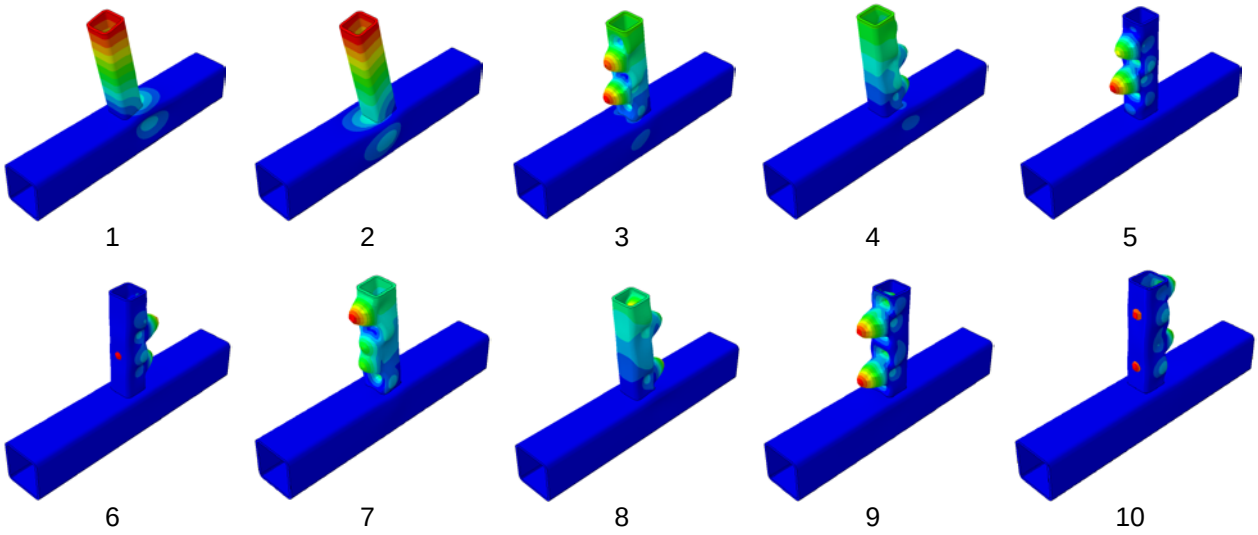

Figure 9. Buckling modes, in-plane bending

The buckling modes for axial loading are provided in Figure 10. A negative Mode 1 represents a buckling mode closest to the real deformation pattern of the joint under an axial load (compare with Figure 4a). Modes 4 and 9 correspond to the lateral buckling of the chord and cannot be used to simulate local imperfections of the cross-section. Modes 5 and 10 are located in the brace. Modes 7 and 8 are similar to Modes 1 and 6, respectively. Mode 3 represents the buckling of the chord side walls in opposite

direction, i.e. inwards the tube. Based on these observations, Modes 1, 2 and 6 were selected as the most reliable for the simulation of imperfections, both in the case of in-plane bending and axial loading.

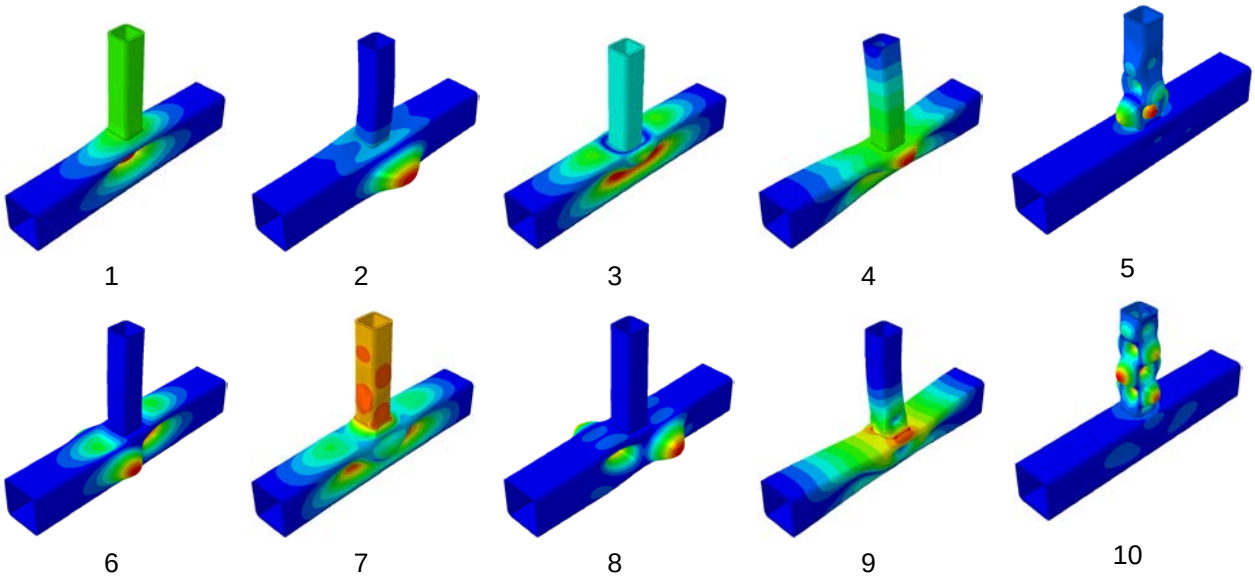

Figure 10. Buckling modes, axial loading

On the second step, a nonlinear static analysis was conducted for the joint separately under in-plane bending and axial loading. The analyses were conducted with and without imperfections. Imperfections were simulated using Modes 1, 2 and 6 for both loading cases. Each buckling mode was first applied independently and then in a combination with others. The combination was introduced according to Eq. (1), employing the following equation:

$$e_0 = e_1 + 0.7e_2 + 0.7e_6 \tag{7}$$

The scaling factors for the buckling modes were selected such that the total convexity on the web e_0 was equal to the assumed limitation of $h_0/125$ = 0.8 mm. Being negative, Mode 1 was applied in the opposite direction. The outcome of the numerical analyses included the plastic resistance and initial stiffness of the analyzed joints. The results are presented in Table 1, where "Imperfect-N" relates to the model with imperfections obtained from a buckling mode *N*. "Imperfect-C" corresponds to the model with imperfections obtained from the combination of buckling modes, Eq. (7). The results are presented in absolute values and in relation to "Perfect" model.

Table 1. Structural behavior of joints with various imperfections

	M_{pl} [kNm]		$S_{j,ini}$ [kNm/rad]		N_{pl} [kN]		$C_{j,ini}$ [kN/mm]	
Perfect	3.15	1	262.0	1	121.9	1	219.9	1
Imperfect-1	3.12	0.99	256.9	0.98	120.1	0.98	210.4	0.96
Imperfect-2	3.15	1.00	262.0	1.00	121.9	1.00	220.0	1.00
Imperfect-6	3.15	1.00	262.1	1.00	122.9	1.01	220.0	1.00
Imperfect-C	3.13	1.00	259.0	0.99	120.8	0.99	214.3	0.97

As can be seen, the influence of initial geometric imperfections on the structural behavior is negligibly small. The reduction of resistance does not exceed 1 % for moment load and 2 % for axial load. For initial stiffness, the values account for 2 % and 4 % respectively. For both loading cases, the most conservative results are observed employing buckling Mode 1, i.e. the mode that as close as possible corresponds to the deformation pattern of the joint under an axial brace loading. This buckling mode can be considered further as the bounding buckling mode. Although in this section it corresponded to the first computed buckling mode, its number can be different for other joints.

3.2. Parametric studies for joints with various geometry and steel grades

This section evaluates the effect of geometric imperfections on the structural behavior of RHS T joints with varying geometries and steel grades. The variations of geometry are considered in relation to chord wall thickness and the width of the brace. As in Section 3.1, firstly a linear buckling analysis was conducted for every joint, followed by a nonlinear static analysis. Initial imperfections were simulated

using the bounding buckling mode that maximally repeats the deformation of the joint under an axial load. The results are evaluated in relation to resistance and initial stiffness, separately under moment and axial loading.

3.2.1. Joints with various steel grade

Consider firstly the effect of steel grade on the behavior of the joint. The analyses were conducted on the same joint as was used in Section 3.1. In addition to S355, the study considered steel grades S500 and S700, employing similar bi-linear material models. The results are presented in Figure 11 and Table 2, where indices *p* and *i* relate to perfect and imperfect models, respectively. As can be seen, the small influence of initial imperfections remains also for higher steel grades. Similarly, imperfections reduce plastic moment and axial resistance by 1 % and 2 % respectively. Initial rotational and axial stiffness is reduced by 2 % and 4 % respectively.

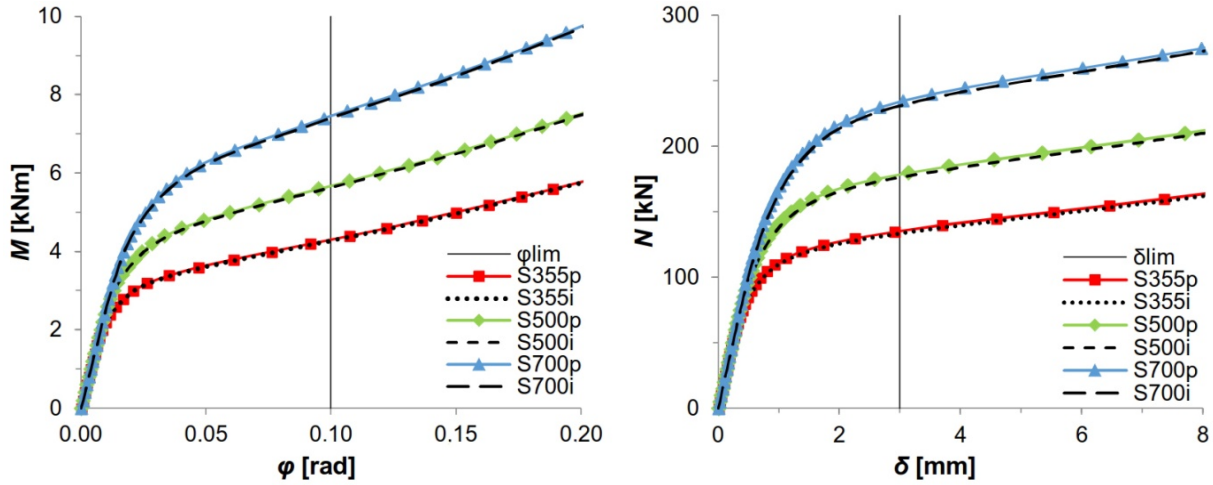

Figure 11. Influence of initial imperfections on joints with various steel grades

Table 2. Influence of initial imperfections for joints with various steel grades

Steel grade	S355p	S355i	S355i/ S355p	S500p	S500i	S500i/ S500p	S700p	S700i	S700i/ S700p
M_{pl} [kNm]	3.15	3.12	0.99	4.26	4.23	0.99	5.73	5.69	0.99
$S_{j,ini}$ [kNm/rad]	262.0	256.9	0.98	262.0	256.9	0.98	262.0	256.9	0.98
N_{pl} [kN]	121.9	120.1	0.98	165.4	162.6	0.98	221.7	218.2	0.98
$C_{j,ini}$ [kN/mm]	219.9	210.4	0.96	219.9	210.4	0.96	219.9	210.4	0.96

3.2.2. Joints with various chord wall thickness

The next parametric study investigates the effect of initial geometric imperfections on the behavior of joints with varying chord wall thickness. Generally, this thickness is characterized by the chord width-to-thickness ratio $\gamma = b_0/2t_0$, which for simplicity is often considered as $2\gamma = b_0/t_0$. Chapter 7 of EN 1993-1-8:2005 [25] limits 2γ in the range of $10 \le 2\gamma \le 35$. Initial geometrical imperfections are known to considerably reduce the resistance of thin-walled members [4]. For this reason, a more pronounced effect can be expected for the joints with 2γ close to its upper limit.

Section 3.1 evaluated the joint with $2\gamma = 100/6 = 16.6$, which is close to the lower bound of γ. In the following, two additional chord thicknesses are considered: $2\gamma = 25.0$ ($t_0 = 4$ mm) and $2\gamma = 33.3$ ($t_0 = 3$ mm). The thickness of the brace was selected as equal to the thickness of the chord. The results are presented graphically in Figure 12 and collected in Table 3, where indices *p* and *i* relate to perfect and imperfect models, respectively. As can be seen, the effect of initial imperfections is more pronounced for joints with thinner walls, reducing their moment and axial resistance by 3 % for $2\gamma = 33.3$. A more pronounced infunence is observed for initial stiffness: rotational stiffness is reduced by 4 %, while axial stiffness is reduced by 6 %.

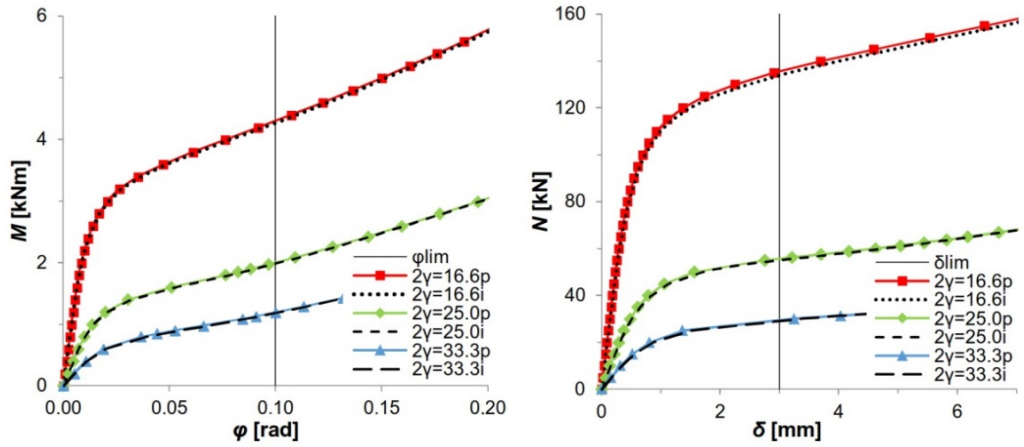

Figure 12. Influence of initial imperfections on joints with various chord wall thickness

Table 3. Influence of initial imperfections for joints with various chord wall thickness

2γ	16.6p	16.6i	16.6i/ 16.6p	25.0p	25.0i	25.0i/ 25.0p	33.3p	33.3i	33.3i/ 33.3p
M_{pl} [kNm]	3.15	3.12	0.99	1.29	1.27	0.98	0.67	0.65	0.97
$S_{j,ini}$ [kNm/rad]	262.0	256.9	0.98	86.4	84.1	0.97	39.6	38.1	0.96
N_{pl} [kN]	121.9	120.1	0.98	48.8	47.9	0.98	25.0	24.3	0.97
$C_{j,ini}$ [kN/mm]	219.9	210.4	0.96	70.9	67.6	0.95	31.9	30.1	0.94

3.3. Joints with various brace width

The third and the last parametric study evaluates the influence of initial imperfections of joints with different brace widths. Generally, the brace width is represented by the brace-to-chord width ratio β. EN 1993-1-8:2005 [25] limits β for RHS T joints in the range of $0.25 \leq \beta \leq 1.0$. All previous analyses considered the joints with $\beta = 0.6$ and demonstrated a negligibly small effect of initial imperfections. Although this finding can be justified for the joints that fail from chord face bending, the results can differ for the joints with other failure modes, e.g. chord side walls buckling, which is critical when $0.85 < \beta \leq 1.0$.

Consider the structural behavior of equal-width joints ($\beta = 1.0$). The analyses were conducted for a joint with a 100x100 chord and a 100x100 brace, made of S355, with three chord wall thicknesses: $2\gamma = 16.6$ ($t_0 = 6$ mm), $2\gamma = 25.0$ ($t_0 = 4$ mm) and $2\gamma = 33.3$ ($t_0 = 3$ mm). The wall thickness of the brace was selected as equal to the wall thickness of the chord. The resistance of the joints was determined according to Figure 8. The structural behavior of the joints is illustrated in Figure 13 and summarized in Table 4, where indices *p* and *i* relate to perfect and imperfect models, respectively. As can be seen, the negative influence of initial imperfections observed for joints with $\beta = 0.6$ remains also for equal-width joints. Similarly, the effect is more pronounced for the joints with thinner walls, reducing their moment and axial resistance by 2% and 5% respectively for $2\gamma = 33.3$. In relation to initial stiffness, the reducing effect does not exceed 7%. It should be noted that the effect is more pronounced for axial loading than for in-plane bending.

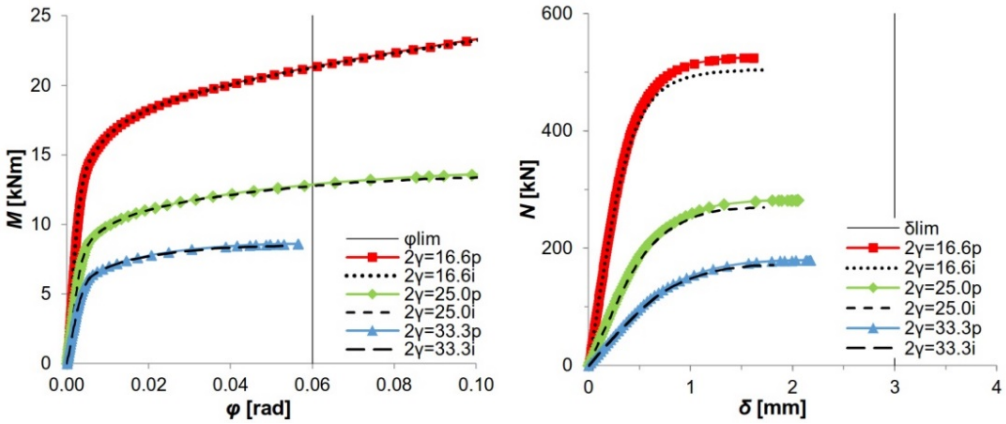

Figure 13. Influence of initial imperfections on joints with $\beta = 1.0$

Table 4. Influence of initial imperfections on joints with β = 1.0

2γ	16.6p	16.6i	16.6i/ 16.6p	25.0p	25.0i	25.0i/ 25.0p	33.3p	33.3i	33.3i/ 33.3p
M_{pl} [kNm]	21.34	21.29	1.00	12.85	12.77	0.99	8.61	8.44	0.98
$S_{j,ini}$ [kNm/rad]	4281	4237	0.99	2332	2295	0.98	1578	1538	0.97
N_{pl} [kN]	525.3	503.7	0.96	282.0	269.3	0.95	179.9	171.2	0.95
$C_{j,ini}$ [kN/mm]	1181	1102	0.93	429	403	0.94	213	201	0.94

3.4. Discussion

In this paper, geometrical imperfections were modelled applying scaled buckling modes to the perfect geometry. Buckling modes were obtained from linear buckling analyses for the corresponding loading type. The comparative buckling analyses under axial loading have showed that the first buckling mode most closely corresponds to the deformation pattern of T joints, being thus the most desirable for the simulation of initial imperfections. The consideration of higher buckling modes as well as their possible combinations brought no noticeable changes in further results and therefore was found unnecessary. At the same time, all buckling modes resulted from in-plane bending loading were located in the brace and therefore could not be employed to simulate local deformations of the chord walls. For this reason, imperfections for both loading cases were modelled using the first buckling mode obtained from axial loading. This resulted to the fact that the observed influence of imperfections was less pronounced for in-plane bending than for axial loading. In all cases studied in this paper, the first buckling mode was negative and was multiplied by a negative scaling factor to be applied in the proper direction.

The conducted parametric studies have demonstrated a small negative influence of initial imperfections on both design resistance and initial stiffness of the investigated joints. The effect was observed for the joints governed by chord face bending ($\beta \leq 0.85$) as well as the joints with chord side walls buckling as the dominating failure mode ($\beta > 0.85$). The structural properties were found to decrease for the joints with thinner walls, particularly those with 2γ ratio close to its upper limit specified by the Eurocode ($2\gamma = 35$). For the joints beyond this limit ($2\gamma > 35$), the effect is expected to be more pronounced, making these joints behave similar to thin-walled sections. At the same time, the negative effect of imperfections showed no correlation with steel grade in the considered range from S355 to S700.

The maximum observed reduction of resistance accounted 3 % and 5 % for in-plane bending moment and axial loading respectively. In practice, these reductions are taken into account by partial safety factors and thus do not have to be considered in theoretical calculations. At the same time, initial imperfections reduce initial rotational stiffness by 4 % and initial axial stiffness by 7 %. Since the accuracy requirements for initial stiffness are not as strict as for resistance, these small reductions of stiffness are acceptable and can be ignored in the design. It should be noted that in this paper imperfections were modelled rather conservatively, using the maximum allowed value of $h_0/125$. The experimental measurements of on RHS tubes [5, 29, 30] demonstrate that real imperfections are generally smaller than this amplitude. Moreover, imperfections were applied in the most unfavorable way, i.e. providing the most unsafe behavior. In real members, the distribution of imperfections is more random. These findings allow to conclude that initial geometrical imperfections do not seriously affect the structural behavior of RHS T joints in the range defined by the regulations of the Eurocode.

4. Conclusions

This paper analyzed the effect of initial geometric imperfections on the structural behavior of tubular joints. In this study, initial geometrical imperfections were simulated using the conventional approach for thin-walled sections, applying corresponding buckling modes scaled in accordance with allowable fabrication tolerances. The comparative FE analyses for RHS joints with perfect and imperfect geometry have showed that the effect of initial geometric imperfections on the strength of joints is smaller than that observed for thin-walled cold-formed structures. For this reason, geometrical imperfections can be neglected in the design of RHS T joints with no serious consequences on their design results.

The presented results can serve as a starting point for studying the issue of initial imperfections in relation to welded tubular joints. This paper considered the joints that follow the requirements of Eurocode, i.e. $0.25 \leq \beta \leq 1.0$, $10 \leq 2\gamma \leq 35$, steel grades from S355 to S700, under in-plane bending and axial loading. For joints with $\beta \leq 0.85$, chord face bending governs the deformation of the joint under all loading cases; therefore, the obtained conclusions can be extended also for the case of out-of-plane bending. Some comparative numerical analyses can be conducted to eliminate a possible scaling effect,

considering joints with different sections of the chord. Moreover, some calculations can be useful to extend the conclusions for other welded connections, including K and X joints, as well as circular hollow section joints. In addition, particularly important results can be obtained considering geometrical imperfections in welds, i.e., the deviations of fillet welds from their nominal dimensions.

References

1. *European Committee for Standardization (CEN). Eurocode 3.* Design of steel structures. Part 1-6: Strength and Stability of Shell Structures (EN 1993-1-6:2007). Brussels, 2007.
2. Brar G.S., Singh C.S. FEA of residual stress in cruciform welded joint of hollow sectional tubes. *Journal of Constructional Steel Research.* 2014. Vol. 102. Pp. 44–58.
3. Moradi Eshkafti M. *Influence of various welding sequence schemes on the load bearing capacity of square hollow section T-joint.* PhD thesis. Cottbus: Brandenburg University of Technology, 2017.
4. Dubina D., Ungureanu V., Landolfo R. *Design of Cold-formed Steel Structures: Eurocode 3: Design of Steel Structures, Part 1-3: Design of Cold-formed Steel Structures* . ECCS, 2012.
5. Jiao H., Zhao X.-L. Imperfection, residual stress and yield slenderness limit of very high strength (VHS) circular steel tubes. *Journal of Constructional Steel Research.* 2003. Vol. 59. No. 2. Pp. 233–249.
6. Feldmann M., Schillo N., Schaffrath S., Virdi K., Björk T., Tuominen N., Veljkovic M., Pavlovic M., Manoleas P., Heinisuo M., Mela K., Ongelin P., Valkonen I., Minkkinen J., Erkkilä J., Pétursson E., Clarin M., Seyr A., Horváth L., Kövesdi B., Turán P., Somodi B. *Rules on high strength steel.* Luxembourg: Publications Office of the European Union, 2016.
7. Pavlenko A.D., Rybakov V.A., Pikht A.V., Mikhailov E.S. Non-uniform torsion of thin-walled open-section multi-span beams. *Magazine of Civil Engineering.* 2016. Vol. 67, No. 7. Pp. 55–69.
8. de Matos R.M.M.P., Costa-Neves L.F., de Lima L.R.O., Vellasco P.C.G.S., da Silva J.G.S. Resistance and elastic stiffness of RHS “T” joints: Part I - Axial brace loading. *Latin American Journal of Solids and Structures.* 2015. Vol. 12. No. 11. Pp. 2159–2179.
9. Christitsas A.D., Pachoumis D.T., Kalfas C.N., Galoussis E.G. FEM analysis of conventional and square bird-beak SHS joint subject to in-plane bending moment — experimental study. *Journal of Constructional Steel Research.* 2007. Vol. 63. No. 10. Pp. 1361–1372.
10. Tusnina O.A., Danilov A.I. The stiffness of rigid joints of beam with hollow section column. *Magazine of Civil Engineering.* 2016. Vol. 64. No. 4. Pp. 40–51.
11. Nazmeeva T.V., Vatin N.I. Numerical investigations of notched C-profile compressed members with initial imperfections. Magazine of Civil Engineering. 2016. Vol. 62. No. 2. Pp. 92–101.
12. Zeinoddini V., Schafer B.W. Global Imperfections And Dimensional Variations In Cold-Formed Steel Members. *International Journal of Structural Stability and Dynamics*. 2011. Vol. 11. No. 5. Pp. 829–854.
13. Garifullin M., Pajunen S., Mela K., Heinisuo M., Havula J. Initial in-plane rotational stiffness of welded RHS T joints with axial force in main member. *Journal of Constructional Steel Research.* 2017. Vol. 139. Pp. 353–362.
14. *Abaqus 6.12.* Getting Started with Abaqus: Interactive Edition . Dassault Systèmes, 695 p., 2012.
15. *European Committee for Standardization (CEN). Cold formed welded structural hollow sections of non-alloy and fine grain steels.* Part 2: Tolerances, dimensions and sectional properties (EN 10219-2:2006). Brussels, 2006.
16. van der Vegte G.J., Makino Y. Further research on chord length and boundary conditions of CHS T- and X-joints. *Advanced Steel Construction.* 2010. Vol. 6. No. 3.

Литература

1. European Committee for Standardization (CEN). Eurocode 3. Design of steel structures. Part 1-6: Strength and Stability of Shell Structures (EN 1993-1-6:2007). Brussels, 2007.
2. Brar G.S., Singh C.S. FEA of residual stress in cruciform welded joint of hollow sectional tubes // Journal of Constructional Steel Research. 2014. Vol. 102. Pp. 44–58.
3. Moradi Eshkafti M. Influence of various welding sequence schemes on the load bearing capacity of square hollow section T-joint. PhD thesis . Cottbus: Brandenburg University of Technology, 2017.
4. Dubina D., Ungureanu V., Landolfo R. Design of Cold-formed Steel Structures: Eurocode 3: Design of Steel Structures, Part 1-3: Design of Cold-formed Steel Structures . ECCS, 2012.
5. Jiao H., Zhao X.-L. Imperfection, residual stress and yield slenderness limit of very high strength (VHS) circular steel tubes // Journal of Constructional Steel Research. 2003. Vol. 59. № 2. Pp. 233–249.
6. Feldmann M., Schillo N., Schaffrath S., Virdi K., Björk T., Tuominen N., Veljkovic M., Pavlovic M., Manoleas P., Heinisuo M., Mela K., Ongelin P., Valkonen I., Minkkinen J., Erkkilä J., Pétursson E., Clarin M., Seyr A., Horváth L., Kövesdi B., Turán P., Somodi B. Rules on high strength steel. Luxembourg: Publications Office of the European Union, 2016.
7. Павленко А.Д., Рыбаков В.А., Пихт А.В., Михайлов Е.С. Стесненное кручение многопролетных тонкостенных балок открытого профиля // Инженерно-строительный журнал. 2016. № 7(67). С. 55–69
8. de Matos R.M.M.P., Costa-Neves L.F., de Lima L.R.O., Vellasco P.C.G.S., da Silva J.G.S. Resistance and elastic stiffness of RHS “T” joints: Part I - Axial brace loading // Latin American Journal of Solids and Structures. 2015. Vol. 12. № 11. Pp. 2159–2179.
9. Christitsas A.D., Pachoumis D.T., Kalfas C.N., Galoussis E.G. FEM analysis of conventional and square bird-beak SHS joint subject to in-plane bending moment — experimental study // Journal of Constructional Steel Research. 2007. Vol. 63. № 10. Pp. 1361–1372.
10. Туснина О.А., Данилов А.И. Жесткость рамных узлов сопряжения ригеля с колонной коробчатого сечения // Инженерно-строительный журнал. 2016. № 4(64). С. 40–51.
11. Назмеева Т.В., Ватин Н.И. Численные исследования сжатых элементов из холодногнутого просечного С-профиля с учетом начальных несовершенств // Инженерно-строительный журнал. 2016. № 2(62). С. 92–101.
12. Zeinoddini V., Schafer B.W. Global Imperfections And Dimensional Variations In Cold-Formed Steel Members // International Journal of Structural Stability and Dynamics. 2011. Vol. 11. № 5. Pp. 829–854.
13. Garifullin M., Pajunen S., Mela K., Heinisuo M., Havula J. Initial in-plane rotational stiffness of welded RHS T joints with axial force in main member // Journal of Constructional Steel Research. 2017. Vol. 139. Pp. 353–362.
14. Abaqus 6.12. Getting Started with Abaqus: Interactive Edition . Dassault Systèmes, 695 p., 2012.
15. European Committee for Standardization (CEN). Cold formed welded structural hollow sections of non-alloy and fine grain steels. Part 2: Tolerances, dimensions and sectional properties (EN 10219-2:2006) . Brussels, 2006.
16. van der Vegte G.J., Makino Y. Further research on chord

Garifullin M., Bronzova M., Heinisuo M., Mela K., Pajunen S. Cold-formed RHS T joints with initial geometrical imperfections. *Magazine of Civil Engineering*. 2018. No. 4(80). Pp. 81–94. doi: 10.18720/MCE.80.8

Pp. 879–890.

17. van der Vegte G.J., Wardenier J., Puthli R.S. FE analysis for welded hollow-section joints and bolted joints. *Proceedings of the Institution of Civil Engineers — Structures and Buildings.* 2010. Vol. 163. No. SB6. Pp. 427–437.
18. AlHendi H., Celikag M. Behavior of reverse-channel and double-reverse-channel connections to tubular columns with HSS. *Journal of Constructional Steel Research*. 2015. Vol. 112. Pp. 271–281.
19. *European Committee for Standardization (CEN). Eurocode 3.* Design of steel structures. Part 1-5: Plated structural elements (EN 1993-1-5:2006). Brussels, 2006.
20. Packer J., Puthli R., van der Vegte G.J., Wardenier J. Discussion on the paper “Experimental and numerical assessment of RHS T-joints subjected to brace and chord axial forces”, by Nizer et al., Steel Construction 9 (2016), No. 4, pages 315–322. *Steel Construction.* 2017. Vol. 10. No. 1. Pp. 89–90.
21. Tran A.T., Veljkovic M., Rebelo C., da Silva L.S. Resistance of cold-formed high strength steel circular and polygonal sections - Part 2: Numerical investigations. *Journal of Constructional Steel Research.* 2016. Vol. 125. Pp. 227–238.
22. Zhao X., Tootkaboni M., Schafer B.W. Laser-based cross-section measurement of cold-formed steel members: Model reconstruction and application. *Thin-Walled Structures.* 2017. Vol. 120. Pp. 70–80.
23. Schafer B.W., Peköz T. Computational modeling of cold-formed steel: characterizing geometric imperfections and residual stresses. *Journal of Constructional Steel Research.* 1998. Vol. 47. Pp. 193–210.
24. Rybakov V.A., Al Ali M., Panteleev A.P., Fedotova K.A., Smirnov A. V. Bearing capacity of rafter systems made of steel thin-walled structures in attic roofs. Magazine of Civil Engineering. 2017. Vol. 76. No. 8. Pp. 28–39.
25. *European Committee for Standardization (CEN). Eurocode 3.* Design of steel structures, Part 1–8: Design of joints (EN 1993-1-8:2005). Brussels, 2005.
26. Hoang V.L., Demonceau J.-F., Jaspart J.-P. Resistance of through-plate component in beam-to-column joints with circular hollow columns. *Journal of Constructional Steel Research.* 2014. Vol. 92. Pp. 79–89.
27. Pavlovčič L., Detzel A., Kuhlmann U., Beg D. Shear resistance of longitudinally stiffened panels-Part 1: Tests and numerical analysis of imperfections. *Journal of Constructional Steel Research.* 2007. Vol. 63. Pp. 337–350.
28. Ongelin P., Valkonen I. *SSAB Domex Tube. Structural hollow sections.* EN 1993 - Handbook 2016. SSAB Europe Oy, 2016.
29. Hayeck M., Nseir J., Saloumi E., Boissonnade N. Experimental characterization of steel tubular beam-columns resistance by means of the Overall Interaction Concept. *Thin-Walled Structures*. 2017. Vol. In press.
30. Ellobody E., Young B. Structural performance of cold-formed high strength stainless steel columns. *Journal of Constructional Steel Research.* 2005. Vol. 61. No. 12. Pp. 1631–1649.
31. Garifullin M., Pajunen S., Mela K., Heinisuo M. 3D component method for welded tubular T joints. *Tubular Structures XVI – Proceedings of the 16th International Symposium on Tubular Structures (ISTS 2017).* Melbourne, Australia, 2017 / ed. Heidarpour A., Zhao X.-L. London: Taylor & Francis Group, 2018. Pp. 165–173.
32. Lu L.H., de Winkel G.D., Yu Y., Wardenier J. Deformation limit for the ultimate strength of hollow section joints. *Tubular Structures VI. 6th International Symposium on Tubular Structures.* Melbourne, Australia / ed. Grundy P.,

length and boundary conditions of CHS T- and X-joints // Advanced Steel Construction. 2010. Vol. 6, No. 3. Pp. 879–890.

17. van der Vegte G.J., Wardenier J., Puthli R.S. FE analysis for welded hollow-section joints and bolted joints. Proceedings of the Institution of Civil Engineers — Structures and Buildings. 2010. Vol. 163, No. SB6. Pp. 427–437.
18. AlHendi H., Celikag M. Behavior of reverse-channel and double-reverse-channel connections to tubular columns with HSS. Journal of Constructional Steel Research. 2015. Vol. 112. Pp. 271–281.
19. European Committee for Standardization (CEN). Eurocode 3. Design of steel structures. Part 1-5: Plated structural elements (EN 1993-1-5:2006) . Brussels, 2006.
20. Packer J., Puthli R., van der Vegte G.J., Wardenier J. Discussion on the paper “Experimental and numerical assessment of RHS T-joints subjected to brace and chord axial forces”, by Nizer et al. Steel Construction 9 (2016), No. 4, pages 315–322 // Steel Construction. 2017. Vol. 10, № 1. Pp. 89–90.
21. Tran A.T., Veljkovic M., Rebelo C., da Silva L.S. Resistance of cold-formed high strength steel circular and polygonal sections - Part 2: Numerical investigations // Journal of Constructional Steel Research. 2016. Vol. 125. Pp. 227–238.
22. Zhao X., Tootkaboni M., Schafer B.W. Laser-based cross-section measurement of cold-formed steel members: Model reconstruction and application // Thin-Walled Structures. 2017. Vol. 120. Pp. 70–80.
23. Schafer B.W., Peköz T. Computational modeling of cold-formed steel: characterizing geometric imperfections and residual stresses // Journal of Constructional Steel Research. 1998. Vol. 47. Pp. 193–210.
24. Рыбаков В.А., Ал Али М., Пантелеев А.П., Федотова К.А., Смирнов А.В. Несущая способность стропильных систем из стальных тонкостенных конструкций в чердачных крышах // Инженерно-строительный журнал. 2018. № 8(76). С. 28–39.
25. European Committee for Standardization (CEN). Eurocode 3. Design of steel structures, Part 1–8: Design of joints (EN 1993-1-8:2005) . Brussels, 2005.
26. Hoang V.L., Demonceau J.-F., Jaspart J.-P. Resistance of through-plate component in beam-to-column joints with circular hollow columns // Journal of Constructional Steel Research. 2014. Vol. 92. Pp. 79–89.
27. Pavlovčič L., Detzel A., Kuhlmann U., Beg D. Shear resistance of longitudinally stiffened panels-Part 1: Tests and numerical analysis of imperfections // Journal of Constructional Steel Research. 2007. Vol. 63. Pp. 337–350.
28. Ongelin P., Valkonen I. SSAB Domex Tube. Structural hollow sections. EN 1993 - Handbook 2016 . SSAB Europe Oy, 2016.
29. Hayeck M., Nseir J., Saloumi E., Boissonnade N. Experimental characterization of steel tubular beam-columns resistance by means of the Overall Interaction Concept // Thin-Walled Structures. 2017. Vol. In press.
30. Ellobody E., Young B. Structural performance of cold-formed high strength stainless steel columns // Journal of Constructional Steel Research. 2005. Vol. 61. № 12. Pp. 1631–1649.
31. Garifullin M., Pajunen S., Mela K., Heinisuo M. 3D component method for welded tubular T joints // Tubular Structures XVI – Proceedings of the 16th International Symposium on Tubular Structures (ISTS 2017). Melbourne, Australia, 2017 / ed. Heidarpour A., Zhao X.-L. London: Taylor & Francis Group, 2018. Pp. 165–173.
32. Lu L.H., de Winkel G.D., Yu Y., Wardenier J. Deformation

Гарифуллин М.Р., Бронзова М.К., Хейнисуо М., Мэла К., Паюнен С. Сварные узлы холодногнутых труб прямоугольного сечения с начальными несовершенствами // Инженерно-строительный журнал. 2018. № 4(80). С. 81–94.

Holgate A., Wong B. Rotterdam: Balkema, 1994. Pp. 341–347.

33. Zhao X.-L., Hancock G.J. T-joints in rectangular hollow sections subject to combined actions. *Journal of Structural Engineering.* 1991. Vol. 117. No. 8. Pp. 2258–2277.
34. Grotmann D., Sedlacek G. *Rotational stiffness of welded RHS beam-to-column joints.* Cidect 5BB-8/98 . Aachen: RWTH-Aachen, 1998.
35. Zhao X.-L. Deformation limit and ultimate strength of welded T-joints in cold-formed RHS sections. *Journal of Constructional Steel Research.* 2000. Vol. 53. No. 2. Pp. 149–165.

limit for the ultimate strength of hollow section joints // Tubular Structures VI. 6th International Symposium on Tubular Structures. Melbourne, Australia / ed. Grundy P., Holgate A., Wong B. Rotterdam: Balkema, 1994. Pp. 341–347.

33. Zhao X.-L., Hancock G.J. T-joints in rectangular hollow sections subject to combined actions // Journal of Structural Engineering. 1991. Vol. 117. № 8. Pp. 2258–2277.
34. Grotmann D., Sedlacek G. Rotational stiffness of welded RHS beam-to-column joints. Cidect 5BB-8/98 . Aachen: RWTH-Aachen, 1998.
35. Zhao X.-L. Deformation limit and ultimate strength of welded T-joints in cold-formed RHS sections // Journal of Constructional Steel Research. 2000. Vol. 53. № 2. Pp. 149–165.

Marsel Garifullin,*
+7(999)034-60-70; marsel.garifullin@tut.fi

Maria Bronzova,
+7(921)330-25-29; bronzochka@mail.ru

Markku Heinisuo,
+358(40)596-58-26; markku.heinisuo@tut.fi

Kristo Mela,
+358(40)849-05-63; kristo.mela@tut.fi

Sami Pajunen,
+358(40)849-05-71; sami.pajunen@tut.fi

Марсель Ринатович Гарифуллин,*
+7(999)034-60-70;
эл. почта: marsel.garifullin@tut.fi

Мария Константиновна Бронзова,
+7(921)330-25-29;
эл. почта: bronzochka@mail.ru

Маркку Хейнисуо,
+358(40)596-58-26;
эл. почта: markku.heinisuo@tut.fi

Кристо Мэла,
+358(40)849-05-63; эл. почта: kristo.mela@tut.fi

Сами Паюнен,
+358(40)849-05-71;
эл. почта: sami.pajunen@tut.fi

Garifullin M., Bronzova M., Heinisuo M., Mela K., Pajunen S. Cold-formed RHS T joints with initial geometrical imperfections. *Magazine of Civil Engineering*. 2018. No. 4(80). Pp. 81–94. doi: 10.18720/MCE.80.8